Fracture and Weakening of Jammed Subduction Shear Zones, Leading to the Generation of Slow Slip Events

Adam Beall[1], Åke Fagereng[1] and Susan Ellis[2]

[1]School of Earth and Ocean Sciences, Cardiff University, Cardiff, UK
[2]GNS Science, Avalon, Lower Hutt, New Zealand

Key Points:

- Fracturing of clasts in a mélange with viscosity contrasts of 10^3 occurs at applied stresses 80% lower than for a homogeneous fault
- Fracturing of clasts in load-bearing force chains leads to stress redistribution into the viscously creeping matrix
- A transient reduction in clast strength by 75% can increase mélange strain-rate by 8×, potentially generating a slow slip event

Corresponding author: Adam Beall, `bealla1@cardiff.ac.uk`

Abstract

Geodetic data have revealed that parts of subduction interfaces creep steadily or transiently. Transient slow slip events (SSEs) are typically interpreted as aseismic frictional sliding. However, SSEs may also occur via mixed visco-brittle deformation, as observed in exhumed shear zones containing mixtures (mélange) of strong fractured clasts embedded in a weak visco-brittle matrix. We test the hypothesis that creep in a subduction mélange occurs through distributed matrix deformation, where flow is modified and impeded by load-bearing clast networks. Our numerical models demonstrate that bulk mélange rheology can be dominated by the strong clasts in the absence of fracturing, while at high driving stresses or low frictional strength, clast fracturing redistributes deformation into the matrix, leading to high bulk strain-rates. Mélange stress is highly heterogeneous, fracturing some clasts even when the bulk mélange stresses are only 20% of the clast yield strength, though with minor strain-rate increase due to clast stress redistribution. Transient strain-rate increases have previously been modelled as periods of lowered frictional strength. Mélange clasts must weaken significantly ($\sim 75\%$) in order to increase strain-rate by 8x. Frictional weakening could occur through the formation of extension or extensional-shear fractures in clasts, as observed within shear networks in exhumed mélange outcrops. We outline a model where high bulk strain-rates are generated when pervasive fracturing occurs, but further slip is limited by viscous processes. Incorporating such viscous damping into models may widen the conditions under which SSEs can occur while preventing development of seismic slip.

Plain Language Summary

While some subduction zones are responsible for generating large, devastating earthquakes, others creep steadily or episodically. This range of deformation styles may correspond to the varying interaction of viscous creep and frictional failure, as observed in exhumed subduction shear zones, which are typically mixtures (mélanges) of strong fractured and weak viscous materials. We use computer models to explore how mélange strength and deformation style varies when the frictional material fractures. Load-bearing networks of unfractured strong material contribute significantly to mélange strength, so the onset of fracturing redistributes some deformation into the weak viscous material. As the force distribution in these networks is complicated, the onset of frictional failure alone is insufficient to completely unload the strong material. However, if the frictional ma-

terial weakens considerably, as may occur when fractures open, mélange may undergo a period of rapid, predominately viscous deformation. Cycles of viscous deformation may correspond to episodic creep events. If creep events do occur primarily by a viscous mechanism, this may explain why they can occur routinely in some regions without transitioning to seismic slip.

1 Introduction

The rheology and frictional properties of the subduction thrust interface exert a first-order control on the generation of major earthquakes (Scholz, 1998) and the maximum sustainable stresses and deformation rates at a convergent margin (Duarte et al., 2015; Behr & Becker, 2018). The down-dip limit of a subduction thrust seismogenic zone is often thought to be limited by the onset of steady viscous creep at temperatures $>350^o$ (e.g. Hyndman et al., 1997). Slow slip events (SSEs), episodes of aseismic slip $\sim$0.1 - 1 m/year (faster than plate velocities) and commonly associated with tectonic tremor, have been observed in this transition zone (Rogers & Dragert, 2003; Schwartz & Rokosky, 2007). These events require an evolution in our understanding of the gradual spatial transition between the seismogenic zone and deeper, steady aseismic creep. SSEs have been primarily considered to arise due to frictional dynamics (Liu & Rice, 2005; Leeman et al., 2018). It has also been proposed that SSEs are the result of dynamic interaction between viscous and frictional deformation (Ando et al., 2012; Fagereng et al., 2014; Hayman & Lavier, 2014), though it is still unclear which visco-brittle rheological model is most appropriate.

Mélange, a mixture of strong clasts embedded in a weak matrix, is commonly found in exhumed subduction-related shear zones and in some places preserves a mixture of contemporaneously formed brittle and ductile structures resulting from the interplay between strong (brittle) clasts and weak (ductile) matrix (Fagereng & Sibson, 2010). Matrix deformation is typically distributed, likely as a result of a predominately creeping process such as pressure solution, as observed at the μm scale in fine-grained phyllosilicates, quartz and calcite, in combination with dilation of frictionally weak phyllosilicate cleavage (Bos & Spiers, 2001; Kitamura et al., 2005; Rowe et al., 2011; Wassmann & Stöckhert, 2013; Fagereng & den Hartog, 2016). Such pressure solution may be responsible for subduction interface creep. Fractures within the mélange, predominately found in clasts, are indicative of locally high strength and stress (in the absence of extreme pore pressure variation). Depending on the connectivity of these high stress clasts, there may be no connected matrix pathways for simple shear to occur, in which case the mélange rheology will be strong (referred to as jammed) and dependent on clast fracturing. Such load-bearing networks are called force chains and their reorganisation is responsible for stick-slip events in granular materials (Hayman et al., 2011). As a result of force chain dynamics, the observed viscous and brittle mélange deformation may preserve cycles of alternating deformation mechanisms, perhaps generating SSEs.

Viscous creep, for example pressure solution of quartz, can stabilise sliding along adjacent frictional minerals (Niemeijer, 2018), producing velocity-strengthening behaviour. Velocity-strengthening parts of a subduction interface can produce an SSE by dampening an otherwise unstable rupture initiating in velocity-weakening material (Skarbek et al., 2012; Luo & Ampuero, 2018). Analogue models show that slow stick-slip events can occur in a macroscopically homogeneous viscoplastic material likely due to reorganisation of microgel force chains (Reber et al., 2015; Birren & Reber, 2019). Microscopically, these events are related to reorganisation of force chains, while macroscopically they correspond to episodic opening of tensile fractures, which grade into shear fractures and viscous deformation accommodating overall simple shear. In contrast, slow stick-slip events have been produced in rock experiments at normal stresses of < 10 MPa and high (>0.9) apparatus to critical stiffness ratios (Kaproth & Marone, 2013; Scuderi et al., 2017; Leeman et al., 2018). Visco-brittle interactions are difficult to quantify in such experiments, but microstructural observations indicate that frictional instabilities occur when deformation localizes in shear bands, and slip style may be controlled by the interplay between the rheology of such shear bands and the surrounding fault rock (Scuderi et al., 2017). It is, however, still unclear if ductile and brittle interactions are necessary to produce strain-rate transients such as SSEs, and if rheological interactions do occur, what are the fundamental processes and scales at which they operate.

Mélange rheology can be dominated by weak matrix constituents if there are connected matrix shear pathways that accommodate bulk simple shear (Handy, 1994). However, finite element models (Webber et al., 2018; Beall et al., 2019) demonstrate that minor shear strain of mélange with around 50% or more ellipsoidal clasts leads to the formation of clast force chains which block matrix pathways (Fig. 1a), switch the mélange to clast-dominated deformation (jamming), and consequently decrease strain-rate by more than an order of magnitude. We explore the hypothesis that such force chains may be disabled through the fracturing of clasts as their yield strength is reached after jamming (Fig. 1b), which redistributes stress into the matrix. This increase in matrix stress would consequently increase the bulk shear zone strain-rate. If this hypothesis is correct, mélange deformation would temporarily switch between being limited by frictional failure and being controlled by viscous creep, as proposed in previous models (Lavier et al., 2013; Reber et al., 2015). Geological evidence for such visco-brittle interaction indicates this process could occur from centimetre up to 100s of metre scales (Fagereng & Sibson, 2010; Fagereng, 2011a; Rowe et al., 2011; Grigull et al., 2012; Hayman & Lavier, 2014). To integrate shear zone dynamics into large scale models, mélange deformation must be parameterized into a bulk rheology relating effective stresses to strain-rates and/or strain (see Section 2, below).

Mélange clasts are commonly fractured, despite the low differential stress implied by creep of adjacent matrix. While fracturing is typically thought to indicate near-lithostatic pore-pressure (e.g. Sibson, 1996), Beall et al. (2019) showed that clast shear stress can be increased by $> 3\times$ due to the viscosity contrast between clasts and matrix, even in the absence of a force chain network. These models did not incorporate fracturing, so it is unclear how pervasive fracturing would be and how it affects mélange rheology. Mélange fracture kinematics are typically consistent with matrix simple shear (Fagereng, 2011b). Fractures are also commonly confined to clasts or transition into terminating shear fractures in the matrix (Fisher & Byrne, 1987; Raimbourg et al., 2009; Fagereng, 2013). While these observations support a model of contemporaneous frictional and viscous deformation, it is unclear how frictional failure would affect the bulk mélange rheology. In this study, we incorporate fracturing into our numerical mélange models and quantify both 1) how pervasive clast fracturing is at varying shear zone stress, and 2) whether fracturing could effectively disable force chains and increase shear zone strain-rates.

2 Bulk Rheology of a Subduction Interface: Theoretical Mixture Model Predictions

Geodynamic models of visco-brittle subduction interface deformation typically combine one viscous and one brittle rheology into a composite rheology (Karato, 2012), following the assumption that both rheologies experience either the same stress (the Reuss model) or the same strain (the Voigt model). The choice of Reuss or Voigt model dictates which rheology dominates at low and high stress (Fig. 1c).

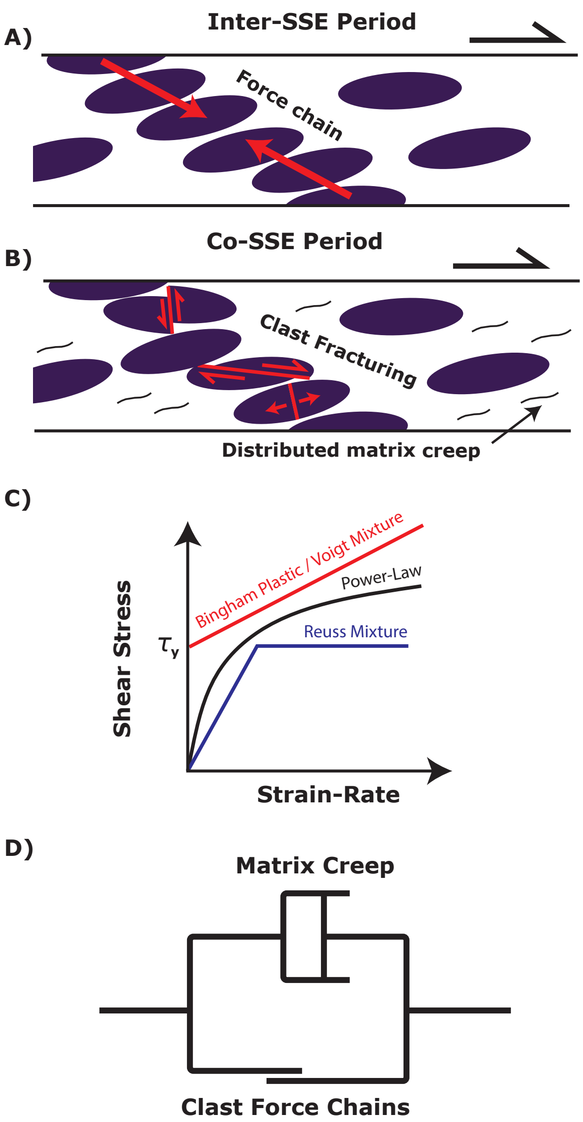

Figure 1. A) Periods of low megathrust creep in-between SSEs are hypothesised to be due to the formation of clast force chains, which prevent viscous matrix deformation. B) When clasts fracture, stress may be redistributed to the weak matrix, switching the mélange to predominately viscous deformation with a high strain-rate. C) Schematic comparison of the Voigt (equivalent to Bingham plastic) and Reuss mixture models (and comparison to power-law rheology). When fracturing begins at $\tau = \tau_y$ (or lower if stress amplification is considered), the Voigt model is rate-limited by viscous deformation, while the Reuss model becomes stress-limited by frictional deformation (which may be modestly rate-strengthening or weakening, or constant as shown here). D) We hypothesise that the rheology of a jammed mélange can be modelled as a viscous dashpot (matrix creep) in parallel with a frictional slider (fracture of clasts, neglecting their slow viscous creep), equivalent to a Bingham plastic.

The Reuss model represents material that can always viscously flow (though slowly for high viscosities), but switch to frictional deformation if a yield stress is reached. For predominately viscous slip transients to occur in a Reuss mixture, the viscous rheology must be highly non-linear (e.g. incorporating shear heating; Goswami & Barbot, 2018). The Voigt model, which is equivalent to a Bingham plastic when one of the materials is frictional (Fig. 1c), represents a material that does not deform at all until frictional sliding occurs, at which point viscous deformation becomes rate-limiting and a low viscosity may produce high strain-rates (used by Ando et al., 2012; Lavier et al., 2013). Stress-dependent viscous deformation is generally captured by the power-law rheology $\dot{\epsilon} \propto \sigma^n$ (Fig. 1c) for maximum shear strain-rate $\dot{\epsilon}$ and stress τ (Karato, 2012). The magnitude of the stress exponent n dictates how stress-dependent the rheology is, for example $n \approx 3$ for dislocation creep and $n \to \infty$ for a plastic material with a yield strength. It is unclear which model best captures the rheology of a subduction interface shear zone.

If a mélange only deforms when clasts in a force chain can deform, then assuming that clast and matrix strain is equal will give the Voigt / Bingham model. This model is supported by GPS records, which generally show that inter-SSE locking is high on interface patches hosting SSEs (e.g. Wallace & Beavan, 2010). If clast and matrix stresses are each homogeneously defined by constants τ_{clast} and τ_{matrix}, their stresses are related to the bulk stress by $\tau = \phi\tau_{clast} + (1 - \phi)\tau_{matrix}$. If clasts are purely frictional, τ_{clast} is limited to a yield stress τ_y, and if τ_{matrix} is controlled by Newtonian viscous creep $2\eta\dot{\epsilon}$ (e.g. pressure solution creep), then an effective rheology is given by Eq. 1, i.e. a Bingham rheology (Fig. 1c-d), where viscous creep occurs if bulk mélange stress $\tau \geq \phi\tau_y$.

$$\tau = \phi\tau_y + 2(1 - \phi)\eta\dot{\epsilon} \tag{1}$$

This simple model predicts that frictional failure and the activation of viscous flow occurs at a bulk stress which is lower than the frictional clast strength, as stress is focussed into only the clast volume (controlled by ϕ). This stress amplification has been shown to occur in models with complex force chain geometries, where frictional yield occurs for bulk stresses well below the clast yield limit due to the clast-matrix viscosity contrast (Beall et al., 2019). Eq. 1 also predicts that the viscous strain-rate will be zero when frictional failure first occurs, as $\tau_{matrix} = 0$ when $\tau = \phi\tau_y$, unless τ_y is dynamically decreased or τ is increased further. Clast stresses are not, however, likely to be homogeneous for realistic force chain geometries and matrix strain-rate will not be completely zero, so the predicted stress for the onset of visco-brittle deformation is an approximate guide.

3 Methodology

The modelling methodology is adapted from Beall et al. (2019), in which a Newtonian viscous mélange was modelled as lens-shaped clasts embedded in a matrix, where the clasts had a viscosity $10-10^4\times$ higher than the matrix. The velocity at the top boundary was derived by applying a constant driving stress, allowing an effective strain-rate and bulk viscosity to be calculated, as well as the mélange stress distribution, as a function of the viscosity contrast, clast proportion ϕ and shear zone thickness. Jamming of mélange with a viscosity contrast of 10^3 resulted in an effective viscosity increase of $2-7\times$ and clast shear stress of $6-9\tau$ (for applied driving stress τ), over the range $0.5 \leq \phi \leq 0.64$. Here, we build upon these previous models by incorporating frictional failure into the clast rheology. This study also follows Webber et al. (2018), though is more simplified in order to characterise mélange rheology in a generalised manner.

Shear zone deformation is modelled as incompressible creeping viscous flow, via the continuum-mechanics finite-element particle-in-cell code Underworld, which solves the Stokes equations. The matrix has a Newtonian viscosity η_m, representing diffusion creep processes such as the pressure solution observed in quartz-phyllosilicate mixtures (Bos & Spiers, 2001; Fagereng & den Hartog, 2016; Niemeijer, 2018) at temperatures of $\geq 100^o$C and within a range of fine-grained metamorphic assemblages at lower crustal conditions (Wassmann & Stöckhert, 2013). Frictional failure is incorporated by checking if each point within the clast material has a maximum shear stress $\tau_{max} = (\sigma_1 - \sigma_2)/2$ (where σ_1 and σ_2 are the in-plane principal stresses) exceeding a frictional strength τ_y, in which case an effective viscosity is iteratively calculated at that point in order to satisfy $\eta_f = \frac{1}{2}\tau_y/\dot{\epsilon}_{max}$ (for maximum shear strain-rate $\dot{\epsilon}_{max}$ at that point in space and time; following Fullsack, 1995; Moresi & Solomatov, 1998). The yield stress is either set to a constant or to the Coulomb failure criteria Eq. 2, for friction coefficient μ, cohesion C and effective mean stress σ_{eff} (Jaeger et al., 2007).

$$\tau_y = \frac{\mu\sigma_{eff} + C}{\sqrt{1+\mu^2}} \tag{2}$$

Table 1. Summary of model-sets and parameters.

Model-set	Frictional Parameters	Clast Proportion (ϕ) and Maximum Width (D_{max})
A	$\mu = 0.7$, $C = 50$MPa ($\tau_y \approx 160$MPa)	$\phi = 0.3$, 0.5, 0.61 ($D_{max} = 0.14$), $\phi = 0.61$ ($D_{max} = 0.28$)
B	$\tau_y = 200$MPa	$\phi = 0.61$ ($D_{max} = 0.14$)
C	$\tau_y = 50$MPa	$\phi = 0.61$ ($D_{max} = 0.14$)

σ_{eff} is calculated as $(p + \rho g z)(1-\lambda)$, where p is a dynamic pressure deviation from the lithostatic pressure, ρ is the average overburden density set to 2650 kg m^{-3}, g is gravitational acceleration, z is depth and λ is the prescribed ratio of pore-pressure to lithostatic pressure. We study deformation at a depth of z =40 km, roughly matching the depth of SSEs in Cascadia (Rogers & Dragert, 2003), southern Hikurangi (Wallace & Beavan, 2010) and the deep SSEs in Nankai (Obara et al., 2004). We assume $\lambda = 0.8$, which is intermediate between hydrostatic and lithostatic (Saffer & Tobin, 2011). This gives $\sigma_{eff} \approx 208$ MPa (when $p = 0$) for the models .

The model dimensions can be rescaled, in order to explore a wider parameter space. We assume that the model stress can be non-dimensionalised as Eq. 3. The accuracy of this scaling should vary depending on the degree to which the bulk strain-rate of the mélange is a function of τ_y. We test the applicability of this scaling for jammed mélange. It then follows that time t (and therefore strain-rate) can be non-dimensionalised as Eq. 4.

$$\tau' = \frac{\tau}{\tau_y} \tag{3}$$

$$t' = t\frac{\tau_y}{\eta_m} \tag{4}$$

We set $\mu = 0.7$ and $C = 50$ MPa, representing frictionally strong clasts (e.g. unfractured sandstone or basalt) close to Byerlee's law (Jaeger et al., 2007). Clast regions which do not meet the failure criterion have a Newtonian viscosity set to $\eta_c = 10^3\eta_m$, representing a large viscosity contrast in the mélange. We also run models with either a high or low constant τ_y in order to explore frictional weakening and test our scaling predictions (parameters summarised in Table 1).

As incompressibility is assumed, deformation involving tensile fracture cannot be calculated, but the onset of tensile failure can be predicted. The calculations with varying τ_y and the scaling approach allow us to explore how mélange rheology depends on clast yield stress, where clast yield includes tensile fracture if it occurs. Tensile failure is assumed to occur when minimum in-plane principal stress $\sigma_2 = T$ for a constant tensile strength T. This tensile yield criterion can be rewritten as Eq. 5.

$$\tau_y = \sigma_{eff} + T \tag{5}$$

At a specific depth, the Coulomb and tensile failure criteria can be approximated by a constant τ_y by assuming that the normal stress is equal to the effective lithostatic pressure (setting $p = 0$). This neglects normal stress variations within the mélange, which are likely to be small compared to the lithostatic pressure for the 40 km depth modelled.

A constant shear traction τ is applied to the top model wall, representing the bulk shear stress to drive deformation (e.g. Webber et al., 2018). A highly viscous Newtonian material with viscosity $10^3\eta_m$ is included in the upper 5% of the model domain, in order to distribute this stress within the underlying mélange. As the bulk rheology of the mélange is of primary interest, a bulk shear strain-rate $\dot{\epsilon}$ is calculated as $0.5V_{av}/L$ for average horizontal velocity on the top wall V_{av} and model height L. We set $L = 100$m, a typical active subduction shear-zone thickness (Rowe et al., 2013) and the model width to $4L$ with periodic boundary conditions. The velocity magnitude is set to zero on the lower boundary. The element resolution is 2048×512, equivalent to a mesh node spacing of 4.9 cm for $L = 100$m.

The ratio of the clast short-axis length to the shear zone width ($L = 100$m) is defined as D. Within most models, D varies from over $0.05 \leq D \leq 0.14$ (labelled as $D_{max} = 0.14$, Table 1). This choice of D_{max} results in a force chain length scale which is smaller than L and therefore a conservative estimate of jamming (Beall et al., 2019). A model with clasts of size $0.1 \leq D \leq 0.28$ is also included ($D_{max} \leq 0.28$) for $\phi = 0.64$, with identical model resolution and dimensions, in order to test whether the choice of D_{max} affects the bulk visco-brittle rheology. All clasts have a short to long axis ratio of 3. Their sizes are chosen to follow a power-law distribution with exponent -2, reflecting clast size distributions in visco-brittle shear zones (Fagereng, 2011a; Grigull et al., 2012). As the clast geometries are fractal (though limited to a minimum clast size due to the limited mesh resolution), the clast sizes can be scaled up to thicker shear zones with larger clasts or down to cm-m scale shear zones. Calculations of stress-strain-rate relationships are therefore scale-invariant, provided our clast geometries and simplified rheologies hold. Such scaling is limited at the large scale by the largest clast dimension (blocks up to 100 m long have been observed; Grigull et al., 2012) and the breakdown of the simplified rheology at the small scale (grain-scale processes are critical at and below the mm scale; Fagereng & den Hartog, 2016).

As the clasts are originally randomly orientated and with minimal force chains present, a setup model is run for each volumetric clast proportion ϕ up to a shear strain of $\epsilon = 2$ to generate a strained mélange with force chains (if ϕ is sufficiently high). This is used as a starting material distribution for the main model experiments. The setup runs neglect clast fracturing, for both computational efficiency (numerical iterations are not required) and to provide identical starting conditions for all models with a given ϕ. The setup strain is sufficient for force chains to form (where ϕ is high enough), though further jamming may occur at higher strain. Mélange formation through disaggregation of stratigraphy and significant simple shear has been inferred to occur before and during lithification (Fagereng, 2011b; Festa et al., 2012). Our initial conditions could therefore apply to any depth.

4 Results

4.1 Simplified Force Chain Model

We firstly test the applicability of Eq. 1, an idealised Voigt (iso-strain) mixture / Bingham rheology, to an idealised numerical model. The visco-brittle clast rheology is assigned to one column orientated at 45^o to the horizontal in the direction of greatest compressive stress. This column represents a force chain, is assigned a constant $\tau_y = 170$ MPa, a width giving $\phi = 0.1$ and is embedded in a viscous matrix (Fig. 2a). Eq. 1 predicts onset of creeping for a bulk stress of 17 MPa. In the numerical model, the instantaneous strain-rate was calculated for a variety of boundary shear stress magnitudes. The simple force chain model almost exactly matches Eq. 1, with the minor exception of a non-zero, though negligible, strain-rate when $\tau < \phi\tau_y$ due to the model clast rheology being viscoplastic rather than perfectly plastic (i.e. in the numerical model creep is allowed when $\tau_{max} < \tau_y$). The Bingham rheology therefore has the potential to capture the bulk rheology of a numerical model when the iso-strain (Voigt) assumption holds. Whether this holds for complicated force chain geometries is explored in the following sections.

4.2 Mélange Fracturing at Low Mélange Boundary Stress

We use Model-set A (Table 1) as a strong end-member to test whether stress-amplification leads to significant fracturing even at bulk stresses much lower than the clast yield stress. For a depth of 40 km, fluid-pressure ratio $\lambda = 0.8$ and in the case that $p = 0$, the frictional parameters for set A give a yield stress $\tau_y = 160$ MPa (Eq. 2). Results show that all models, including for applied stress as low as $\tau = 21$ MPa (non-dimensionalised $\tau' = 0.13$), involved some clast yielding, in which case the clast η_{eff} locally reduces by at least an order of magnitude (in order to satisfy $\tau_{max} = \tau_y$). As we are interested in how fracturing affects dynamics at the shear-zone scale, a better measure of the lower threshold for fracturing is the lowest bulk stress τ modelled for which there is a chain of fracturing clasts spanning L. In this case, fracturing occurs at $\tau \geq 35$ MPa ($\tau' \geq 0.22$, Fig. 3) for $\phi = 0.5$, $D_{max} = 0.28$ and $\phi = 0.61$, $D_{max} = 0.14$, while fracturing requires $\tau \geq 70$ MPa ($\tau' \geq 0.44$) for $\phi = 0.5$ and $\phi = 0.3$, $D_{max} = 0.14$. This shows that significant fracturing can occur when applied stress τ is substantially less than τ_y, particularly for jammed mélange and a volumetric clast proportion $> 50\%$, owing to stress amplification in the clasts.

Clast fracturing occurs at low ratios of driving stress to clast yield stress, $\tau' = 0.22$. The occurrence of fracturing only depends on τ' (as demonstrated in Section 4.4) and can therefore be used to calculate the driving stress τ required to generate fracturing for a specified τ_y, including for tensile failure. Assuming $T = 3.5$ MPa (the ratio of C to T is typically ≈ 15 for sandstone and greater for crystalline rocks; Jaeger et al., 2007), then the corresponding yield stress for tensile failure is $\tau_y = 211$ MPa (Eq. 5). A driving stress of $\tau = 42$ MPa (equivalent to $\tau' = 0.22$), could then generate tensile fracturing. Driving shear stresses of ~ 10 MPa are therefore sufficient to generate shear and/or tensile fracturing of clasts at $z = 40$km when $\lambda = 0.8$ (the dominant fracture mode depending on the orientation of existing weak planes).

The Coulomb failure criterion may be satisfied by shear in two conjugate directions. However, simple shear is expected to be accommodated by sliding predominately along

A)

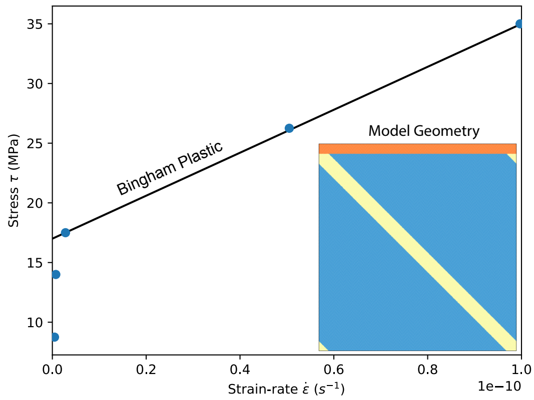

B)

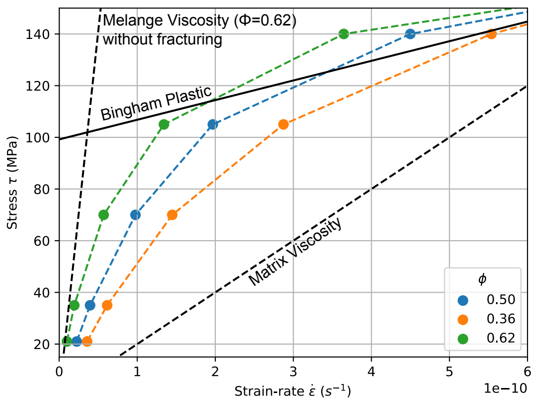

Figure 2. Comparisons of idealised (A) and mélange (B) force chain models to the Bingham plastic rheology. A) Model geometry, inset, of clast material (yellow, $\phi = 0.1$) embedded in matrix (blue) with high viscosity 'grip' material on top (orange). Measurements of τ (points) follow the Bingham plastic rheology (solid line, Eq. 1). B) Model-set A data (for $D_{max} = 14$m), compared to the Bingham rheology and mélange viscosity in the absence of fracturing, for $\phi = 0.62$, as well as η_m.

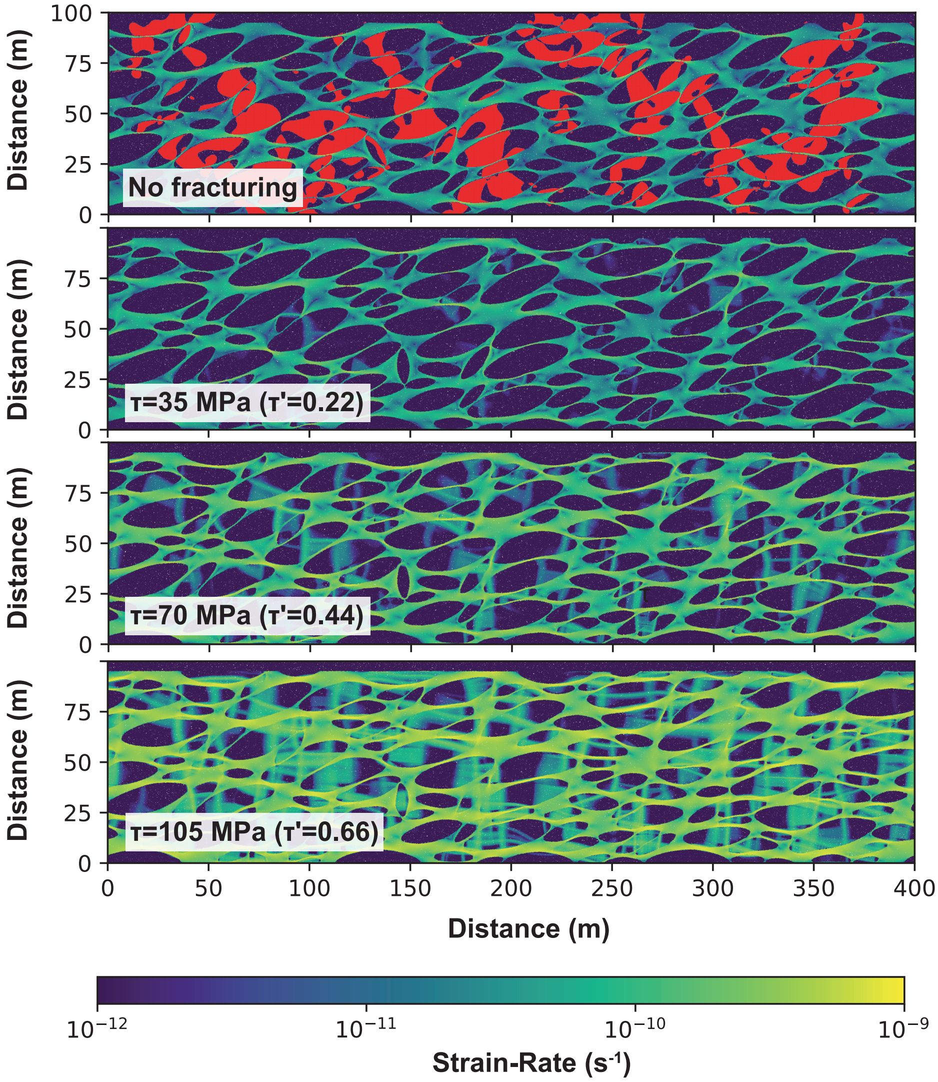

Figure 3. Mélange from model-set A with $\phi = 0.62$, $D_{max} = 14$m and $\eta_m = 10^{17}$ Pa s. For reference, a model with $\tau = 35$ MPa, fracturing prevented and regions with maximum shear stress increased above τ by $\geq 5\times$ colored red. Models with τ varying from 35 to 105 MPa are also shown, demonstrating that the number of clasts reaching the frictional failure criterion increases dramatically with increasing τ and contributes to a significantly higher matrix strain-rate at high τ' compared to a linear rheology.

planes sub-parallel to the shear zone boundary in order to satisfy mass conservation in a homogeneous shear zone with constant thickness. Shear along planes sub-parallel to the shear zone boundary is also the most efficient way of localising simple shear deformation, as no rotation or fracture network is required. Yielding in the models, however, is localised into conjugate sets of failure planes (Fig. 3). Conjugate sets should be symmetrical around σ_1 (which is 45^o clock-wise from the shear zone boundary for the dextral shear sense modelled), which is generally observed in the models (with minor deviation due to stress rotation). In contrast to a homogeneous incompressible material, the shear failure accommodates pure shear of the clasts, which are extended in the direction of σ_2, as evident in the final clast geometries. Localised pure shear of the clasts occurs in the incompressible model because it is compensated by simple shear within the viscous matrix.

The Coulomb failure criteria predicts that failure will predominately occur on planes orientated at angles $\pm tan^{-1}(\mu)/2 = \pm 17.5^o$ to σ_1. Numerical models only reproduce this Coulomb failure angle when a high resolution is used relative to initial stress perturbations and shear bands (Kaus, 2010), otherwise shear failure occurs on planes orientated closer to $\pm 45^o$ to σ_1 (called the Roscoe angles). Yielding zones localise in our models due to the pressure-dependence of the Coulomb criteria, however are still relatively broad ($< 10m$) as no strain softening was incorporated. Failure occurs along bands orientated at a range of angles between the Coulomb and Roscoe angles. The deviation from the Coulomb angles may be due to the mesh resolution being too coarse in places to sufficiently resolve stresses inside the clasts, though this deviation should not significantly affect clast deformation or stress magnitude.

4.3 General Mélange Rheology

Each model in model-set A (Table 1) was repeated with the imposed stress boundary condition varying through $\tau = 21$, 35, 70 and 140 MPa, in order to characterise the effective mélange rheology (Figs. 2b and 4). The models share some of the characteristics of the Bingham rheology; at low applied stress the effective mélange viscosity can be much higher than η_m ($< 15\times$ for these models, depending on ϕ) and at high applied stress the behaviour is dominated by viscous matrix deformation (the slope $d\tau/d\dot{\epsilon}$ is similar to that of the Bingham plastic prediction in Fig. 2b). However, for $\phi = 0.61$ and $\tau = 70$ MPa the fracturing causes the bulk strain-rate to be about $2\times$ higher than ex-

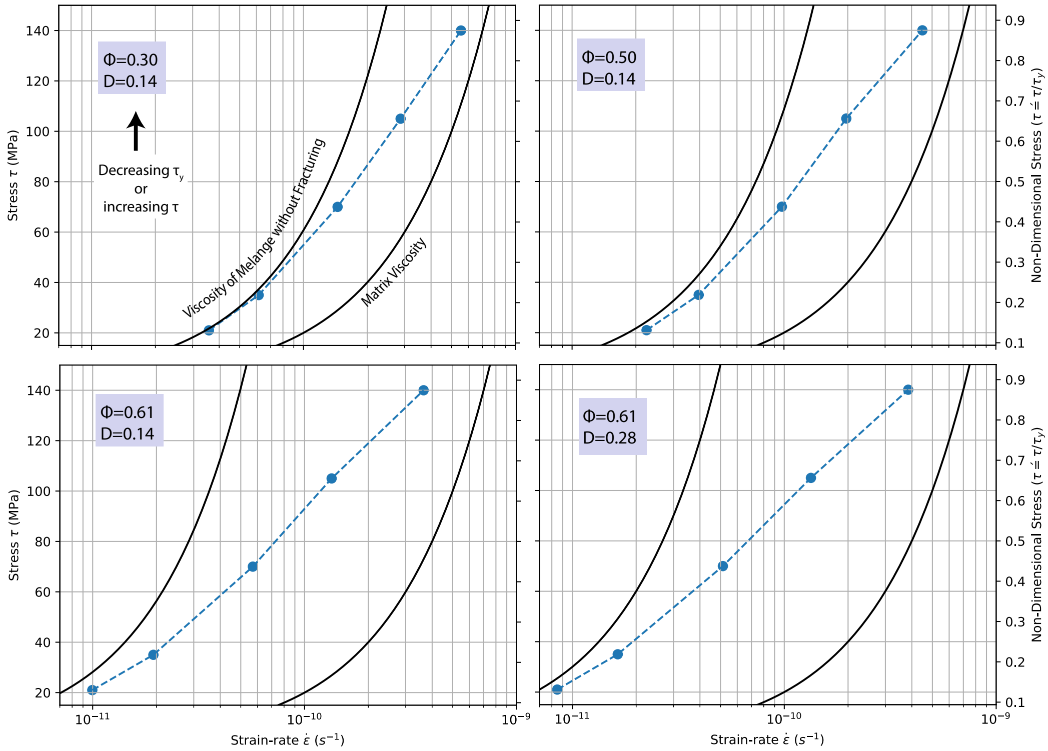

Figure 4. Rheologies of the models in model-set A, demonstrating that strain-rate increases exponentially with stress with a viscosity spanning that of mélange without fracturing at low τ, to η_m at high τ. The highest and lowest jamming occurs for $\phi = 0.61$ and 0.30 respectively, which correspond to the highest and lowest strain-rate variation.

pected for the jammed mélange. This heralds a transition to predominately visco-brittle deformation, which occurs at a lower stress than the 100 MPa predicted for the simplified Bingham rheology. This is due to the heterogeneous stress distribution in the clasts, compared to the homogeneous stress assumed in the simplified model.

While the Bingham rheology is dominated by its viscous constituent when fracturing occurs, the corresponding mélange rheology at high stress is non-Newtonian and strain-rate increases exponentially with stress (i.e τ appears to be logarithmically dependent on $\dot{\epsilon}$) for $\tau \geq 35$ MPa ($\tau' = 0.22$). Accordingly, fitting a power-law relationship of $\dot{\epsilon} \propto \sigma^n$ (though an exponential form provides a superior fit) gives $n \sim 2$, rather than the $n > 10$ that would correspond to a highly non-linear rheology appropriate for a Reuss mixture.

Mélange viscosity should always be greater or equal to the matrix viscosity when $\tau \leq \tau_y$ and less or equal to an identical mélange in which fracturing is prohibited (i.e. a model without frictional failure incorporated). These limits represent the strength end-members (solid black curves, Fig. 4). All of the model bulk rheologies, regardless of ϕ, follow a similar transition from one approximating the strong end-member (no fracturing) at the lowest τ (21 MPa or $\tau' = 0.13$), to resembling the weak end-member (matrix-dominated) for $\tau' \approx 0.75 - 0.9$ (the higher end of the range for greater ϕ). This rheological trend demonstrates that all mélange models, regardless of jamming, are weakened by fracturing even when $\tau < \tau_y$. While the bulk behaviour is bounded by the fracturing-free and clast-free viscosity end-members, fracturing of a jammed mélange results in higher strain-rate variation compared to these limiting cases (Fig. 4).

The exponential rheology $\tau \propto ln(\dot{\epsilon})$ arises because stress is not homogeneously distributed across force chains. The probability distribution of clast points with a particular maximum shear stress are shown in Fig. 5 for models with a range of τ. For $\tau =$ 21 and 35 MPa, the most common stress corresponds to the bulk shear stress τ. More clast particles have a stress higher than τ, than those with a stress lower than τ, resulting in a skewed normal distribution. Stresses higher than τ result from stress amplification within force chains, which occurs to a varying degree. The normal distribution shows, for example, that a stress amplification of $2\times$ is more common than $5\times$. Only a small number of force chains therefore fail when $\tau << \tau_y$. For an incremental increase in scaled stress τ' (corresponding to a τ increase or a τ_y decrease), a much higher number of clasts will fracture due to the non-linear stress distribution, resulting in a non-linear rheology. Stress cannot exceed the failure criterion (it has the appearance of doing so only due to the pressure-dependence introduced by μ), so with increasing τ, clast stress becomes more uniform as it is redistributed, resulting in a peak at τ_y in Fig. 5. By $\tau = 70MPa$ ($\tau' = 0.44$), most clasts are likely to be undergoing frictional failure.

4.4 Frictional Weakening and Scaling

Two extra sets of models with $\phi = 0.61$ and a constant yield stress τ_y were run (B and C, Table 1), for $\tau_y = 50$ MPa and $\tau_y = 200MPa$, to explore how the visco-brittle mélange rheology depends on the magnitude of clast frictional strength. These models are used to test the hypothesised scaling relationships Eqns. 3 and 4, which can then be used to rescale the existing models for any τ_y and η_m.

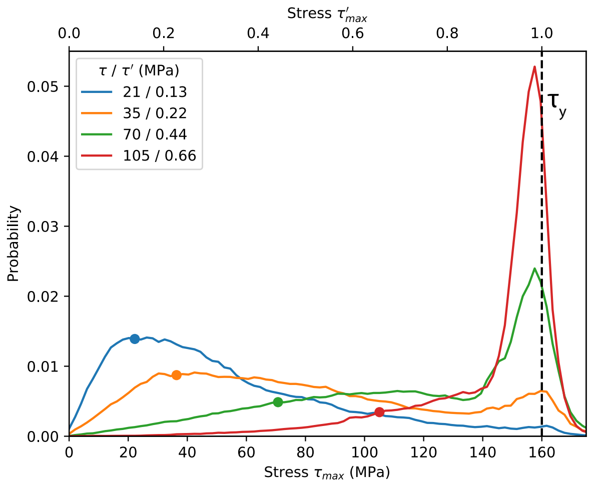

Figure 5. Maximum clast shear stress probability distribution, calculated from all Lagrangian particles identified as clast material, for $\phi = 0.61$, $D_{max} = 14$m. $\tau_y \approx 160$MPa (model-set A) and τ ranging from 21 to 105 MPa (bulk stresses shown by points). At low τ, stress follows a skew normal distribution, capturing heterogeneous stress amplification in force chains. At high τ, stress is limited by τ_y.

When non-dimensionalised, all model-sets with $\phi = 0.61$ collapse onto the same curve as predicted by scaling relations (Fig. 6a). The non-dimensionalised datasets with $\mu = 0$ and $\mu = 0.7$ (pressure independent and dependent τ_y respectively) are identical, indicating that the pressure-dependence of the frictional law and therefore the optimal angle of frictional failure, does not influence the modelled bulk mélange viscosity.

Fig. 6b demonstrates how strain-rate, and therefore velocity at the shear zone wall, would increase if τ_y were decreased for all of the clasts from 200 MPa to 50 MPa. The scaling relationships are also used to calculate an intermediary case of $\tau_y = 80$ MPa. For $\eta_m = 5 \times 10^{17}$Pa s (assumed for Fig. 6b) and $L = 100$m, the average shear zone boundary velocity V_{av} is about 2 cm/yr when $\tau = 50$ MPa and $\tau_y = 200$ MPa. This is equivalent to $\tau' = 0.25$, which is sufficient for fracturing of clasts in the force chains with the highest stress amplification (similar to Fig. 3b). In order to increase the velocity to 4 cm/yr, the clast yield strength needs to be reduced to $\tau_y = 80$ MPa, for example due to extreme strain-weakening as clasts fracture and distribute stress more evenly across the force chains. Should τ_y decrease to $\tau_y = 50$ MPa, the velocity would increase up to 16 cm/yr and the matrix would have a similar stress state to the clasts. This ex-

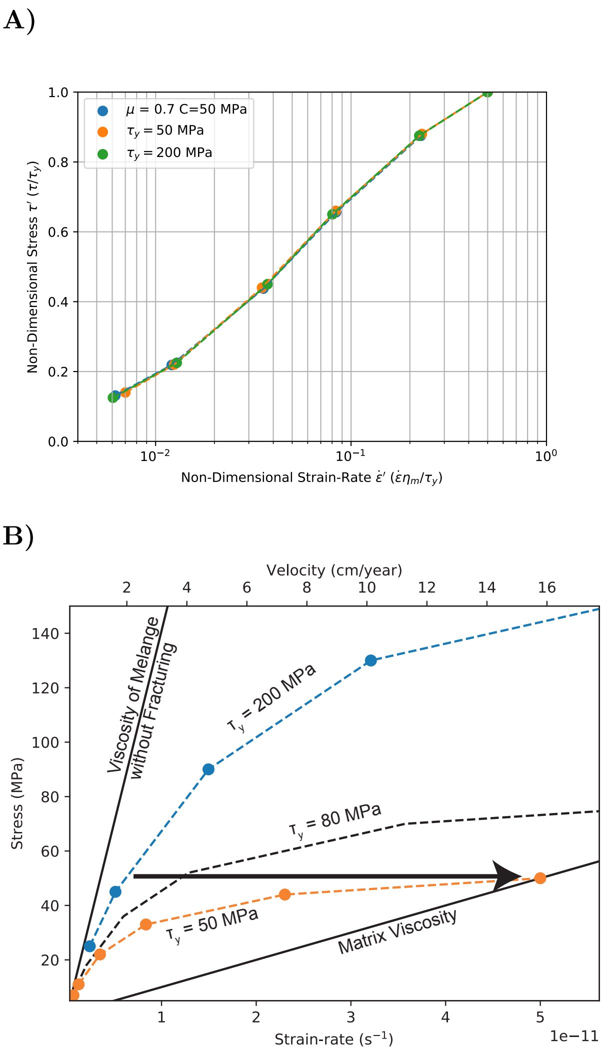

Figure 6. A) Model-sets A-C for $\phi = 0.62$ and $D_{max} = 14$ m, plotted for non-dimensional variables τ' and $\dot{\epsilon}'$ (Eqs. 3 and 4). All data collapses onto one curve, confirming the scaling of stress using τ_y. B) Model sets B and C, with a third case for $\tau_y = 80$ MPa plotting using the scaling relationship and assuming $\eta_m = 5 \times 10^{17}$Pa s. Velocity is calculated assuming $L = 100$ m. In the case of a constant $\tau = 50$ MPa, deformation of mélange containing clasts with a high frictional strength, $\tau_y = 200$ MPa, results in a velocity of 2 cm yr^{-1}. Reducing the clast frictional strength to 50 - 80 MPa (indicated by arrow) would increase this to 4 - 16 cm yr^{-1}.

ample demonstrates that τ' must be initially relatively low in order to generate a large strain-rate transient.

5 Discussion

We previously predicted, and have tested here, that fracturing could occur at relatively low applied shear stress in a mélange due to stress amplification, and this stress amplification could lead to a transient period of high strain-rate until the mélange jams again (Beall et al., 2019, Fig. 1a-b). Fracturing of clasts involved in force chains does indeed occur at low bulk stress, lowering the stress within the most load-bearing force chains. The fracturing also allows surrounding matrix to creep by releasing the jammed portion of the mélange. We found that clast fracturing can occur when $\tau \approx 35$ MPa and $\lambda = 0.8$, even at 40 km depth. More generally, fracturing of multiple force chain clasts (Figs. 3 and 5) occurs when $\tau > 0.22\tau_y$. Fracturing of clasts within a mélange therefore may be just as indicative of a large strength contrast between the matrix and clast minerals, as extreme pore pressure (e.g. Webber et al., 2018).

The models verify that deformation of jammed mélange switches from clast to matrix dominated with increasing bulk stress, as predicted by the Bingham model. In a mixture of strong frictional clasts and weak viscous matrix, mixed visco-brittle deformation may record periods of high stress and/or weakened clasts and therefore high strain-rates (creating slip transients, e.g. SSEs), the duration of which may be related to transient effective stress and healing of fractures. Fracturing at low τ does not, however, result in the dramatic switch to viscous deformation predicted by the Bingham model. This is because clast stresses follow a skew normal distribution and weakening of a force chain with the highest stress amplification does not weaken the force chains with less stress amplification (Fig. 5). This effect does, however, result in a non-linear bulk rheology, as each increment of stress weakens a greater number of force chains at higher stress. The highest strain-rate variation therefore results from changes to the proportion of clasts undergoing frictional failure. As force chains in a jammed material are critically organised, weakening of one force chain will lead to stress redistribution and an entire shear zone can be unjammed if clast weakening is high.

Compared to the weak stress-dependence of frictional sliding, viscous systems are extremely damped (stress-dependent). For example, the viscous strain-rate in a Bingham material increases from zero, when fracturing begins, to $\dot{\epsilon} \propto (\tau - \phi\tau_y)/\eta$ (Eq. 1). A large $\dot{\epsilon}$ therefore requires a large stress increase, large yield stress decrease, or a small viscosity. Ando et al. (2012) inferred that τ_y dynamically decreases by a similar magnitude to the SSE stress drop (typically only 10-100 kPa; Brodsky & Mori, 2007) and as a result predicted an extremely low $\eta_m \sim 10^{11}$ Pa s in order to reproduce SSE velocities. Stress drop in this system, however, could instead be limited by the viscous strain during the SSE and is not necessarily related to τ_y (as would be the case in a Reuss mixture). A large dynamic decrease in τ_y could drive the viscous strain-rate increase. In our models, the frictional clast strength would need to reduce by $\sim 75\%$ to result in an $8\times$ increase in strain-rate (Fig. 6). Should large local variations in τ_y occur, then velocities could transiently increase from 2 up to 16 cm yr^{-1} (plate velocity rates and higher) across a 100 m thick mélange shear zone with $\eta_m = 5 \times 10^{17}$ Pa s for $\tau = 50$MPa (Fig. 6). The predicted matrix viscosity is relatively low, but can be reconciled with pressure-solution creep (Niemeijer, 2018) or phyllosilicate flow laws (Mares & Kronenberg, 1993; Hilairet et al., 2007).

Though the degree of frictional weakening predicted is significantly higher than the $\sim 1\%$ weakening typical of frictional sliding at $\sim 10^{-4}$ m s^{-1} (Marone et al., 1990), it could be explained by opening of extension or extensional-shear fractures in clasts, as an opened fracture becomes a free surface. Such through-going fractures with a tensile component are commonly observed in mélange clasts (Fig. 7a), and can be confined to the clasts and form at an angle of 80^o to discrete shear surfaces parallel to the shear zone S-fabric (Fagereng, 2011b, 2013). These fractures accommodate extension of the clasts (pure shear), which is kinematically consistent with simple shear partitioned into and accommodated by the matrix. The mélange models also deform by this combination of clast pure shear and matrix simple shear. If tensile fracturing were incorporated and favourable over shear failure, the modelled conjugate failure planes would likely be replaced with single tensile fractures. Localised visco-brittle clast deformation grades into distributed viscous matrix deformation in the models, due to the choice of rheologies. These rheologies reflect observed mélange deformation, where fractures within and at the edges of clasts grade into distributed matrix deformation at both thin-section and outcrop scale (Fagereng & Sibson, 2010; Hayman & Lavier, 2014).

Simple shear of mélange may occur by combined deformation of a network of visco-brittle matrix shears and connecting tensile fractures as described in several field examples (Fig. 7b; Sibson, 1996; Meneghini & Moore, 2007; Fagereng et al., 2010; Ujiie et al., 2018). Such shear-fracture meshes within a ductile matrix are analogous to our model, which is rate-limited by viscous deformation when clast fracturing occurs. This model of local fracturing limited by surrounding ductile creep applies when there is no interconnected network of frictional material in the direction of simple shear. In our models, this condition is guaranteed by the assumption of a viscous matrix, however, extrapolation to nature requires that any fractures within the matrix (not modelled here) do not extend/connect to form a more extensive shear fracture network. If localized shears do develop in the matrix, experiments indicate that these may favour development of frictional instabilities, but slip speed is still modulated by their interaction with surrounding creeping matrix (Scuderi et al., 2017).

Stress drop is controlled by the bulk shear zone simple shear strain, which unloads the elastic upper plate. The stress drop in the Bingham model is therefore limited by the magnitude of finite viscous strain during a strain transient, which is limited by the period over which τ_y is weak (i.e. healing). Significant weakening of τ_y does not then necessarily correspond to a large stress drop. Force chain clasts may fracture and weaken, elastically loading the viscous matrix (through elastic strain which was neglected in our models), before regaining their strength at a similar time-scale to viscous creep.

Slow slip events are often modelled as frictional ruptures governed by the empirical rate-and-state laws (Rubin, 2008). In these models, seismic rupture is prevented by the similar strengths of the velocity strengthening and weakening parts, a weak stress-dependence (rate-and-state properties $a - b \approx -10^{-2}$ to -10^{-3}), and the effective normal stress being extremely small (on the order of kPa). A ∼kPa normal stress also implies megathrust shear stresses of similar order, which is difficult to reconcile with estimates of 10 MPa order from geodynamic models (Lamb, 2006) and from creep rheology and piezometry near the brittle-ductile transition (Angiboust et al., 2015). In contrast, in the rheologies used here, provided that the matrix material in the mélange is velocity-strengthening, the strain-rate will always be limited by the matrix viscosity. In our model, the effective normal stress can be ∼10 MPa provided it is low enough so that clast fracturing can occur by local stress amplification (assuming high viscosity contrast and ϕ). Recent rupture models incorporating a microphysical model with viscous creep were able to generate a combination of aseismic and seismic slip events, with an effective normal stress < 50MPa (van den Ende et al., 2018). Incorporating viscous damp-

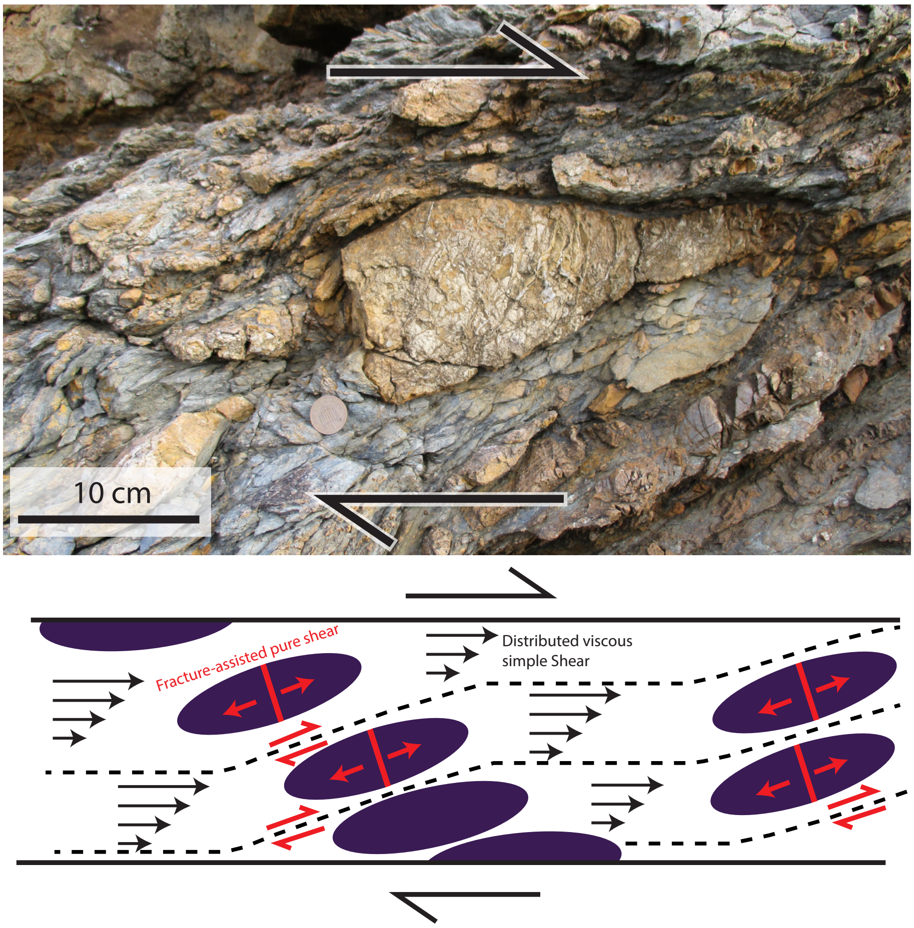

Figure 7. Top) Example of a fractured clast in the Gwna mélange, Cemaes Bay, Anglesey, UK. This is the mélange type locality region (Greenly, 1919) and is interpretted as a subduction accretionary complex (Kawai et al., 2007). Tensile fractures are confined to clasts and are kinematically consistent with distributed matrix shear strain. Bottom) Schematic of hypothesised strain-accumulation mechanisms. Mélange simple shear is accommodated by pure shear of the clasts, which can occur through the opening of extension or extensional-shear fractures, and simple shear within the matrix.

ening into SSE models may therefore be a way to reconcile SSEs with regional stresses of MPas, and help to explain their ubiquity in global subduction zones.

6 Conclusion

We have characterised the bulk rheology of a mélange consisting of strong visco-brittle clasts embedded in a weak viscous matrix using numerical visco-plastic finite element models. When the clasts form a stress-bearing force-chain network, the bulk viscosity of the mélange can be more than an order of magnitude stronger than the matrix viscosity, in the absence of clast fracturing. When fracturing is allowed, clasts within the most load-bearing force chains undergo frictional failure in models with bulk stress far below the clast frictional strength, $\tau \geq 0.22\tau_y$, because of the stress amplification that occurs within a shear zone with high viscosity contrasts. The fracturing of clasts acts to homogenize stress in the force chain network and redistribute stress into viscous matrix deformation. As deformation is limited by clast friction at low stress and rate-strengthening viscous matrix creep at high stress, mélange rheology resembles a Bingham plastic. However, unlike a Bingham plastic, the switch from brittle to viscous deformation occurs across a gradual transition, due to the heterogeneity of force chain stresses. This transition results in an effective rheology in the form of $\dot{\epsilon} \propto ln(\tau)$, as the number of clasts fracturing is more stress-sensitive at higher stress. This gradual transition also requires a large stress increase or clast yield strength decrease ($> 70\%$) in order to produce significant bulk strain-rate increase ($\sim 8\times$).

The models demonstrate how damped (i.e. significantly rate-strengthening) a visco-brittle shear zone can be when no frictional slip surface spans it. Such a damped system could still generate a period of high strain-rate with a negligible stress drop and at $\sim$10 MPa shear stress, if frictionally failing clasts temporarily lose most of their strength. In this case, a matrix viscosity of $< 5\times10^{17}$ Pa s could be reconciled with SSEs, comparable to rheological estimates. We suggest that this frictional weakening could occur due to the opening of extension or extensional-shear fractures. This prediction needs to be tested through future modelling incorporating tensile fracturing and elasticity. Simple shear across the modelled shear zone is accommodated by extension of clasts (pure shear) and simple shear of the matrix. This model is supported by observed shear networks in exhumed mélange. The incorporation of viscous dampening into SSE rupture models is likely to permit aseismic SSEs for a wider range of conditions than presently thought, explaining their ubiquity in subduction zones globally.

Acknowledgments

This project has received funding from the European Research Council (ERC) under the European Union's Horizon 2020 research and innovation program (starting grant agreement 715836 MICA). The Hawk computing cluster (Cardiff University) was used for all numerical calculations. We acknowledge the support of the Supercomputing Wales project, which is part-funded by the European Regional Development Fund (ERDF) via Welsh Government. Ellis was supported by MBIE Endeavour and core research funds to GNS Science. The open-source geodynamic code Underworld is available at http://www.underworldcode.org, and model parameters required to replicate the results are detailed in the manuscript.

References

Ando, R., Takeda, N., & Yamashita, T. (2012). Propagation dynamics of seismic and aseismic slip governed by fault heterogeneity and Newtonian rheology. *Journal of Geophysical Research B: Solid Earth*. doi: 10.1029/2012JB009532

Angiboust, S., Kirsch, J., Oncken, O., Glodny, J., Monié, P., & Rybacki, E. (2015). Probing the transition between seismically coupled and decoupled segments along an ancient subduction interface. *Geochemistry, Geophysics, Geosystems*. doi: 10.1002/2015GC005776

Beall, A., Fagereng, Å., & Ellis, S. (2019). Strength of Strained Two-Phase Mixtures: Application to Rapid Creep and Stress Amplification in Subduction Zone Mélange. *Geophysical Research Letters*. doi: 10.1029/2018GL081252

Behr, W. M., & Becker, T. W. (2018). Sediment control on subduction plate speeds. *Earth and Planetary Science Letters*. doi: 10.1016/j.epsl.2018.08.057

Birren, T., & Reber, J. E. (2019). The impact of rheology on the transition from stick-slip to creep in a semi-brittle analog. *Journal of Geophysical Research: Solid Earth*. doi: 10.1029/2018jb016914

Bos, B., & Spiers, C. J. (2001). Experimental investigation into the microstructural and mechanical evolution of phyllosilicate-bearing fault rock under conditions favouring pressure solution. *Journal of Structural Geology*. doi: 10.1016/S0191-8141(00)00184-X

Brodsky, E. E., & Mori, J. (2007). Creep events slip less than ordinary earthquakes. *Geophysical Research Letters*. doi: 10.1029/2007GL030917

Duarte, J. C., Schellart, W. P., & Cruden, A. R. (2015). How weak is the subduction zone interface? *Geophysical Research Letters*. doi: 10.1002/2014GL062876

Fagereng, Å. (2011a). Frequency-size distribution of competent lenses in a block-in-matrix mélange: Imposed length scales of brittle deformation? *Journal of Geophysical Research: Solid Earth*. doi: 10.1029/2010JB007775

Fagereng, Å. (2011b). Geology of the seismogenic subduction thrust interface. *Geological Society, London, Special Publications*. doi: 10.1144/sp359.4

Fagereng, Å. (2013). On stress and strain in a continuous-discontinuous shear zone undergoing simple shear and volume loss. *Journal of Structural Geology*. doi: 10.1016/j.jsg.2012.02.016

Fagereng, Å., & den Hartog, S. A. M. (2016). Subduction megathrust creep governed by pressure solution and frictional–viscous flow. *Nature Geoscience*. doi: 10.1038/ngeo2857

Fagereng, Å., Hillary, G. W., & Diener, J. F. (2014). Brittle-viscous deformation, slow slip, and tremor. *Geophysical Research Letters*. doi: 10.1002/2014GL060433

Fagereng, Å., Remitti, F., & Sibson, R. H. (2010). Shear veins observed within anisotropic fabric at high angles to the maximum compressive stress. *Nature Geoscience*. doi: 10.1038/ngeo898

Fagereng, Å., & Sibson, R. H. (2010). Mélange rheology and seismic style. *Geology*. doi: 10.1130/G30868.1

Festa, A., Dilek, Y., Pini, G. A., Codegone, G., & Ogata, K. (2012). Mechanisms and processes of stratal disruption and mixing in the development of mélanges and broken formations: Redefining and classifying mélanges. *Tectonophysics*. doi: 10.1016/j.tecto.2012.05.021

Fisher, D., & Byrne, T. (1987). Structural evolution of underthrusted sediments, Kodiak Islands, Alaska. *Tectonics*. doi: 10.1029/TC006i006p00775

Fullsack, P. (1995). An arbitrary Lagrangian-Eulerian formulation for creeping flows and its application in tectonic models. *Geophysical Journal International*. doi: 10.1111/j.1365-246X.1995.tb05908.x

Goswami, A., & Barbot, S. (2018). Slow-slip events in semi-brittle serpentinite fault zones. *Scientific Reports*. doi: 10.1038/s41598-018-24637-z

Greenly, E. (1919). *The geology of Anglesey.* HM Stationery Office.

Grigull, S., Krohe, A., Moos, C., Wassmann, S., & Stöckhert, B. (2012). "Order from chaos": A field-based estimate on bulk rheology of tectonic mélanges formed in subduction zones. *Tectonophysics*. doi: 10.1016/j.tecto.2011.11.004

Handy, M. R. (1994). Flow laws for rocks containing two non-linear viscous phases: A phenomenological approach. *Journal of Structural Geology*. doi: 10.1016/0191-8141(94)90035-3

Hayman, N. W., Ducloué, L., Foco, K. L., & Daniels, K. E. (2011). Granular Controls on Periodicity of Stick-Slip Events: Kinematics and Force-Chains in an Experimental Fault. *Pure and Applied Geophysics*. doi: 10.1007/s00024-011-0269-3

Hayman, N. W., & Lavier, L. L. (2014, mar). The geologic record of deep episodic tremor and slip. *Geology*, *42*(3), 195–198. doi: 10.1130/G34990.1

Hilairet, N., Reynard, B., Wang, Y., Daniel, I., Merkel, S., Nishiyama, N., & Petit-girard, S. (2007). High-pressure creep of serpentine, interseismic deformation, and initiation of subduction. *Science*. doi: 10.1126/science.1148494

Hyndman, R. D., Yamano, M., & Oleskevich, D. A. (1997). The seismogenic zone of subduction thrust faults. *Island Arc*. doi: 10.1111/j.1440-1738.1997.tb00175.x

Jaeger, J. C. J. C., Cook, N. G. W., & Zimmerman, R. W. (2007). *Fundamentals of rock mechanics.* Blackwell Pub.

Kaproth, B. M., & Marone, C. (2013). Slow earthquakes, preseismic velocity changes, and the origin of slow frictional stick-slip. *Science*. doi: 10.1126/science.1239577

Karato, S.-i. (2012). *Deformation of Earth Materials.* doi: 10.1017/cbo9780511804892

Kaus, B. J. (2010). Factors that control the angle of shear bands in geodynamic numerical models of brittle deformation. *Tectonophysics*. doi: 10.1016/j.tecto.2009.08.042

Kawai, T., Windley, B. F., Terabayashi, M., Yamamoto, H., Maruyama, S., Omori, S., ... Isozaki, Y. (2007). Geotectonic framework of the Blueschist Unit on Anglesey-Lleyn, UK, and its role in the development of a Neoproterozoic accretionary orogen. *Precambrian Research*. doi: 10.1016/j.precamres.2006.11.002

Kitamura, Y., Sato, K., Ikesawa, E., Ikehara-Ohmori, K., Kimura, G., Kondo, H., ... Masago, H. (2005). Mélange and its seismogenic roof décollement: A plate boundary fault rock in the subduction zone - An example from the Shimanto Belt, Japan. *Tectonics*. doi: 10.1029/2004TC001635

Lamb, S. (2006). Shear stresses on megathrusts: Implications for mountain building behind subduction zones. *Journal of Geophysical Research*. doi: 10.1029/2005JB003916

Lavier, L. L., Bennett, R. A., & Duddu, R. (2013). Creep events at the brittle ductile transition. *Geochemistry, Geophysics, Geosystems*. doi: 10.1002/ggge.20178

Leeman, J. R., Marone, C., & Saffer, D. M. (2018). Frictional Mechanics of Slow Earthquakes. *Journal of Geophysical Research: Solid Earth*. doi: 10.1029/2018JB015768

Liu, Y., & Rice, J. R. (2005). Aseismic slip transients emerge spontaneously in three-dimensional rate and state modeling of subduction earthquake sequences. *Journal of Geophysical Research: Solid Earth*. doi: 10.1029/2004JB003424

Luo, Y., & Ampuero, J. P. (2018). Stability of faults with heterogeneous friction properties and effective normal stress. *Tectonophysics*. doi: 10.1016/j.tecto.2017.11.006

Mares, V. M., & Kronenberg, A. K. (1993). Experimental deformation of muscovite. *Journal of Structural Geology*. doi: 10.1016/0191-8141(93)90156-5

Marone, C., Raleigh, C. B., & Scholz, C. H. (1990). Frictional behavior and constitutive modeling of simulated fault gouge. *Journal of Geophysical Research*. doi: 10.1029/JB095iB05p07007

Meneghini, F., & Moore, J. C. (2007). Deformation and hydrofracture in a subduction thrust at seismogenic depths: The Rodeo Cove thrust zone, Marin Headlands, California. *Bulletin of the Geological Society of America*. doi: 10.1130/B25807.1

Moresi, L., & Solomatov, V. (1998). Mantle convection with a brittle lithosphere: throughts on the global tectonic styles of the Earth and Venus. *Geophysical Journal International*. doi: 10.1046/j.1365-246X.1998.00521.x

Niemeijer, A. R. (2018, dec). Velocity-dependent slip weakening by the combined operation of pressure solution and foliation development. *Scientific Reports*, *8*(1), 4724. doi: 10.1038/s41598-018-22889-3

Obara, K., Hirose, H., Yamamizu, F., & Kasahara, K. (2004). Episodic slow slip events accompanied by non-volcanic tremors in southwest Japan subduction zone. *Geophysical Research Letters*. doi: 10.1029/2004GL020848

Raimbourg, H., Tadahiro, S., Asuka, Y., Haruka, Y., & Kimura, G. (2009). Horizontal shortening versus vertical loading in accretionary prisms. *Geochemistry, Geophysics, Geosystems*. doi: 10.1029/2008GC002279

Reber, J. E., Lavier, L. L., & Hayman, N. W. (2015). Experimental demonstration of a semi-brittle origin for crustal strain transients. *Nature Geoscience*. doi: 10.1038/ngeo2496

Rogers, G., & Dragert, H. (2003). Episodic tremor and slip on the Cascadia subduction zone: The chatter of silent slip. *Science*. doi: 10.1126/science.1084783

Rowe, C. D., Meneghini, F., & Moore, J. C. (2011). Textural record of the seismic cycle: strain-rate variation in an ancient subduction thrust. *Geological Society, London, Special Publications*. doi: 10.1144/SP359.5

Rowe, C. D., Moore, J. C., & Remitti, F. (2013). The thickness of subduction plate boundary faults from the seafloor into the seismogenic zone. *Geology*. doi: 10.1130/G34556.1

Rubin, A. M. (2008). Episodic slow slip events and rate-and-state friction. *Journal of Geophysical Research: Solid Earth*. doi: 10.1029/2008JB005642

Saffer, D. M., & Tobin, H. J. (2011). Hydrogeology and Mechanics of Subduction Zone Forearcs: Fluid Flow and Pore Pressure. *Annual Review of Earth and Planetary Sciences*. doi: 10.1146/annurev-earth-040610-133408

Scholz, C. H. (1998). *Earthquakes and friction laws.* doi: 10.1038/34097

Schwartz, S. Y., & Rokosky, J. M. (2007). *Slow slip events and seismic tremor at circum-pacific subduction zones.* doi: 10.1029/2006RG000208

Scuderi, M. M., Collettini, C., Viti, C., Tinti, E., & Marone, C. (2017). Evolution of shear fabric in granular fault gouge from stable sliding to stick slip and implications for fault slip mode. *Geology*. doi: 10.1130/G39033.1

Sibson, R. H. (1996). Structural permeability of fluid-driven fault-fracture meshes. *Journal of Structural Geology*. doi: 10.1016/0191-8141(96)00032-6

Skarbek, R. M., Rempel, A. W., & Schmidt, D. A. (2012). Geologic heterogeneity can produce aseismic slip transients. *Geophysical Research Letters*. doi: 10.1029/2012GL053762

Ujiie, K., Saishu, H., Fagereng, Å., Nishiyama, N., Otsubo, M., Masuyama, H., & Kagi, H. (2018). An Explanation of Episodic Tremor and Slow Slip Constrained by Crack-Seal Veins and Viscous Shear in Subduction Mélange. *Geophysical Research Letters*. doi: 10.1029/2018GL078374

van den Ende, M. P., Chen, J., Ampuero, J. P., & Niemeijer, A. R. (2018). A comparison between rate-and-state friction and microphysical models, based on numerical simulations of fault slip. *Tectonophysics*. doi: 10.1016/j.tecto.2017.11.040

Wallace, L. M., & Beavan, J. (2010). Diverse slow slip behavior at the Hikurangi subduction margin, New Zealand. *Journal of Geophysical Research: Solid Earth*. doi: 10.1029/2010JB007717

Wassmann, S., & Stöckhert, B. (2013). *Rheology of the plate interface - Dissolution precipitation creep in high pressure metamorphic rocks.* doi: 10.1016/j.tecto.2013.09.030

Webber, S., Ellis, S., & Fagereng, Å. (2018). "Virtual shear box" experiments of stress and slip cycling within a subduction interface mélange. *Earth and Planetary Science Letters*. doi: 10.1016/j.epsl.2018.01.035